ON THE ROLE OF OIL-FILM BEARINGS IN PROMOTING SHAFT INSTABILITY: SOME EXPERIMENTAL OBSERVATIONS

R.Holmes
School of Engineering and Applied Sciences
University of Sussex,
Falmer, Brighton, Sussex,
U.K. BN1,9QT

SUMMARY

An insight into the mechanism of oil whirl instability is obtained by investigating theoretically and experimentally its occurrence in rigid and flexible rotor systems. Means of damping against such instability are applied in the latter case and their effectiveness discussed.

INTRODUCTION

For a rotating shaft supported in oil-film bearings the instability onset speed depends,to a large extent, on the nature of the hydrodynamic forces produced in the bearings. Oil whirl instability is characterized by shaft vibration frequency and amplitude and the purpose of this paper is to report the effect of various bearing parameters on the oil-whirl frequency and amplitude of rigid and flexible shafts supported on fluid-film bearings.

In order to provide a qualitative understanding of such instability the particular extreme cases of a very short bearing and a very long bearing are considered.

A physical insight into the mechanism of oil-whirl instability can be obtained by considering Fig.1. As a result of the application of an external load the journal deflects on the oil film rather as it would on a spring. Consequently, a converging wedge is formed in the region of contracting film thickness into which oil is dragged by journal rotation, ω. Pressure is thus generated in the oil by hydrodynamic action to counteract the external load. The average angular velocity of this oil is about half rotational speed and, should any disturbance to the journal centre cause the line of centres to rotate at this angular velocity, then the wedge into which the oil is dragged will move away from the oil at the same velocity, with the result that no hydrodynamic pressure will be generated. The journal thus loses its load-carrying capacity and may become unstable in a whirling motion,the energy for the instability being fed by its own rotation.

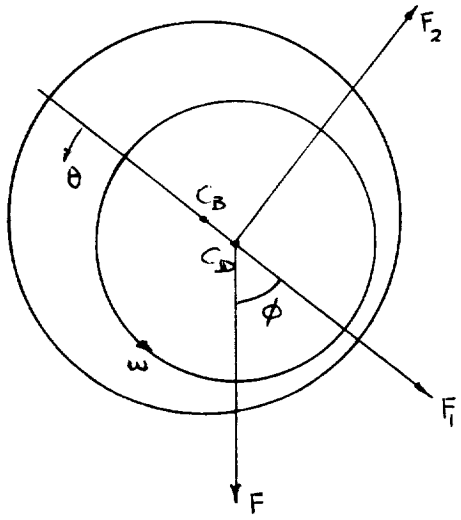

Fig. 1: Forces on journal

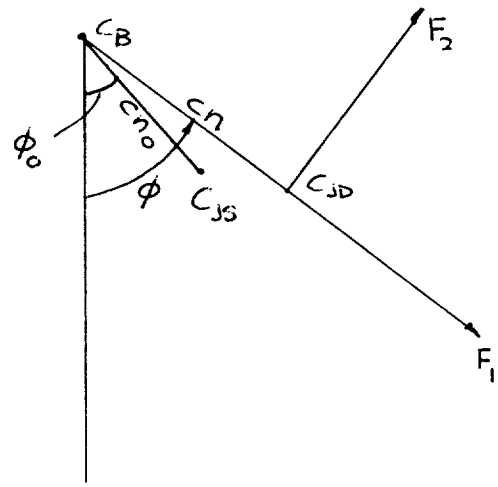

Fig.2: Magnified portion of Fig. 1

NOTATION

a Damper location
b Damping coefficient
c Radial clearance
c_1 Constant
D Diameter
F Static external load per land
F_1, F_2 Oil film forces
g Gravitational constant
h Film thickness at angular co-ordinate $\theta = c(1 + n \cos \theta)$.
inHg Inches of mercury
ℓ Journal length
ℓ_s Shaft span
m Rotor mass per bearing land
n Eccentricity ratio = ε/c
n_o Static eccentricity ratio
p Hydrodynamic pressure
P $F/mc\omega^2$
R = D/2 Journal radius
t Time
z Axial co-ordinate
α Constant
β Constant
ε Eccentricity of journal at instant considered
μ Lubricant viscosity
φ Angle between static load line and line of centres of journal and bearing
ϕ_o Attitude angle under static conditions
ω Journal angular velocity, forcing frequency
Ω Angular velocity of whirl
Ω_1 Lowest pinned critical speed of shaft
$\nu_{D,I} = \frac{b_{D,I}}{m} \left(\frac{c}{g}\right)^{\frac{1}{2}}$ where $b_{D,I}$ is external or internal damping
(') $d/d(\omega t)$

Centres

C_B	Bearing centre
C_{JD}	Centre of dynamic journal at instant considered
C_{JS}	Centre of journal under static load only

Load numbers

$L_{2\pi}$	Load number for long 360^o film $= Fc^2/2\ell\mu\omega R^3$.
$S_{2\pi}$	Load number for short 360^o film $= 4\pi Fc^2/\mu R\ell^3\omega$

THEORETICAL TREATMENT

In the region of diverging film boundaries the hydrodynamic pressure becomes negative and, should the supply pressure be insufficient to maintain a net pressure in the oil of greater than absolute zero then cavitation will usually result. However, in some cases of lightly loaded bearings a full 360^o film of oil is maintained. Not unexpectedly, the spring-like and damping properties of the oil film depend to a large extent on the degree of cavitation present. The equation which governs the generation of hydrodynamic pressure is due to Osborne Reynolds and cannot be solved analytically for the journal bearing situation. However, if one of two approximations is made then a analytical solution is obtainable. These approximations are based on the assumptions that the oil film length in relation to its diameter is (1) very short and (2) very long. These solutions give a good insight into the characteristics of journal bearing oil films. The hydrodynamic forces generated by the short uncavitated oil film (Fig.1) are (Ref.1)

$$F_1 = \frac{-R\ell^3}{c^3}\mu c\dot{n}\cdot\frac{\pi(1+2n^2)}{(1-n^2)^{5/2}}$$

$$F_2 = R\ell^3\,\pi cn\mu(\omega - 2\dot{\phi})/2c^3(1-n^2)^{3/2}$$

Under conditions of static load,

$\frac{dn}{dt}$ and $\dot{\phi}$ are zero, $n = n_o$ and thus

$$F_1 = 0$$

$$F_2 = R\ell^3\pi cn_o\mu\omega/2c^3(1-n_o^2)^{3/2}$$

Also, $F_2 = F$ and $\phi = \pi/2$ (Fig.1).

Therefore $2\pi^2 n_o/(1-n_o^2)^{3/2} = 4\pi Fc^2/\mu R\ell^3\omega$

Let $4\pi Fc^2/\mu R\ell^3\omega$ be called the 'short 2π' load number, given the symbol $S_{2\pi}$.

In terms of static eccentricity ratio, n_o and static load, F, F_1 and F_2 (Fig.2) become

$$F_1 = -2F(1-n_o^2)^{3/2}(1+2n^2)\dot{n}/\omega n_o(1-n^2)^{5/2}$$

and

$$F_2 = F(\omega - 2\dot{\phi})(1-n_o^2)^{3/2}n/\omega n_o(1-n^2)^{3/2}$$

the corresponding expressions for the long bearing are as follows:

$$\begin{Bmatrix} F_1 \\ F_2 \end{Bmatrix} = \frac{36\pi^2 n_o F}{(2+n_o^2)(1-n_o^2)^{\frac{1}{2}}} \begin{Bmatrix} -\frac{\dot{n}}{\omega} \cdot \frac{1}{(1-n^2)^{3/2}} \\ (1-\frac{2\dot{\phi}}{\omega}) \cdot \frac{n}{(2+n^2)(1-n^2)^{\frac{1}{2}}} \end{Bmatrix}$$

and a 'long 2π' load number may be defined having the value

$$L_{2\pi} = \frac{Fc^2}{2\mu R^3 \ell\omega} = \frac{6\pi n_o}{(2+n_o^2)(1-n_o^2)^{\frac{1}{2}}} = \frac{S_{2\pi}}{2\pi} \cdot (\frac{\ell}{D})^2$$

NON-LINEAR EQUATIONS OF RIGID ROTOR MOTION

Consider a symmetrical rigid rotor of mass 2m symmetrically supported on two similar, full-film bearings. From Fig. 1 the equations of motion are

$$F_1 + F\cos\phi = mc(\ddot{n} - n\dot{\phi}^2)$$

$$F_2 - F\sin\phi = mc(n\ddot{\phi} + 2\dot{n}\dot{\phi})$$

These equations become, in non-dimensional form,

$$\frac{F_1}{mc\omega^2} + P\cos\phi = n'' - n\phi'^2$$

$$\frac{F_2}{mc\omega^2} - P\sin\phi = n\phi'' + 2n'\phi' \qquad (1)$$

where $P = F/mc\omega^2$ and $n' = dn/d(\omega t)$ etc.

The following general conclusions may be made from the numerical solutions of equations (1), which result in unstable transient spirals (Fig.3):

(1) The number of loops within a given radius of the static equilibrium position is governed to a large extent by the value of P, the number of loops increasing with rising values of P. A similar less pronounced effect is noted as n_o decreases. Roughly similar numbers of loops are produced by either theory until the bearing centre is enclosed. After this point, the orbits tend to close up and the short bearing solution does so much more rapidly.

The shape of the initial loops is largely dictated by the value of n_o. In general, as n_o is increased, these loops become elongated in the direction of the external load and ultimately may assume a crescent form. Although not restricted to the short bearing solution this distortion is far more pronounced for the case of the short bearing solution than for the long.

Another general conclusion of some interest is that for both the long and short bearing theories the whirl frequency approaches half rotational speed as the eccentricity ratio approaches unity, this approach being at an ever-decreasing rate.

(2) The magnitude of the initial displacement used to commence the solutions has a pronounced effect on the position of loops for solutions having few loops, for example, for low values of P. This effect becomes less apparent as the value of P is increased.

Some general considerations of the equations of motion

One of the main interests attached to the non-linear equations of motion is whether they predict the possibility of a closed orbital motion of the journal centre within the clearance circle. A closed circular orbit concentric with the bearing centre is not possible except for the hypothetical case of a massless rotor, since $\dot{n}$ and hence F_1 and F_2 would be zero, giving no force to counteract the centrifugal force of this postulated whirl. From digital computation with a wide range of parameters it appears that if any other form of closed orbit exists it will occur as $n \to 1$, $n' \to 0$ and $\phi' \to 0.5$. As an approximation these trends were placed in the equations of motion (1).

Experiment

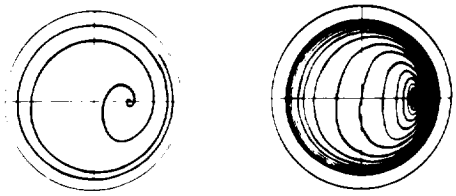

Short bearing theory

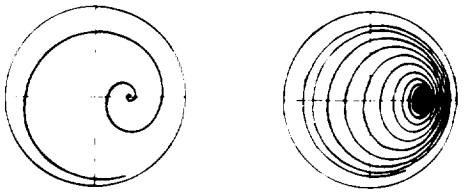

Long bearing theory

Fig.3: Experimental and theoretical transients.

Left-hand column
P = 0.2, n_o = 0.4

Right-hand column
P = 2.5, n_o = 0.6

These give on integration

$$n \simeq 1 - \frac{1}{\left\{c_1+\alpha(\beta-1)\left[\frac{\omega t}{4P} + 2\sin\frac{\omega t}{2}\right]\right\}^{1/(\beta-1)}}$$

c_1 being a constant of integration and $\beta = 2.5$ (short) and 1.5 (long).

Thus n asymptotically approaches unity and it appears that, in general, closed orbits are not possible for $t < \infty$, with the exception of the particular case of $P = \infty$ when the integral oscillates between fixed limits. This corresponds to the massless rotor of Swift (ref.3). It may be seen that dn/dt is curbed more rapidly as n increases, since the exponent β is greater than unity. Further, since β is larger for the short bearing than for the long bearing the curbing for the former is the more pronounced.

Experimental rotor

The motion of an experimental rotor was monitored by pick-ups mounted in the horizontal and vertical planes of the rotor axis and located midway between the bearings. This motion was displayed on a storage oscilloscope and the stored trace was photographed directly when required. This technique allowed the clearance circle to be conveniently displayed by rolling the rotor within the bearing shells. On increasing the rotor speed from zero, an eccentricity locus was traced out on the oscilloscope until the attitude angle ϕ_o reached 90^o, when the rotor became unstable. In view of the low supply pressure in relation to the load pressure this suggested the presence of an oil film supporting sub-atmospheric pressures. In order that different values of P could be inspected, oils of different viscosities were used. This ensured different whirl-onset speeds. When it was required that values of P should be small (high whirl-onset speeds), then the rotor was run up to the required speeds with the supply pressure at approximately 0.5 inHg, being suddenly increased to 6 inHg to give a 90^o attitude angle and to initiate whirl. Some comparisons of experimental results with the equivalent short and long bearing solutions are shown in Fig. 3. For the case of low P, it may be observed that the photograph shows a small white area corresponding to an attitude angle between 0^o and 90^o. This represents a running condition which occurred due to starving the bearings of oil prior to imposing the full supply pressure of 6 inHg. In both the photographs the outer circle denotes the clearance circle. Pick-up non-linearities and the necessary pedestal clamping forces probably contribute to the non-circularity of this clearance circle.

In this experimental work, not only are the initial conditions unknown but they may correspond to an appreciable disturbance for low values of P. Hence although qualitative behaviour may be determined using such values, those likely to show some quantitative agreement with theory are for higher values of P, these being largely unaffected by the initial conditions. Such a case is that corresponding to $P = 2.5$, $n_o = 0.6$.

Bearing these comments in mind, the experimental results support the theoretical solutions in the following respects:

(1) The number of loops increases as P is increased for a given value of n_o. A similar less pronounced effect is obtained on reduction of n_o for a given P.

(2) As n_o is increased, the loops become elongated in the external load direction and can even assume a crescent form.

(3) As the whirl develops the loops become roughly circular in form around the bearing centre.

There is also a general tendency to support the short bearing theory for the initial growth pattern and final decay pattern while the intermediate loops, particularly in distribution, approximate more closely to the long bearing solutions.

One important difference between the computed and experimental spirals is that the former tend to have slightly fewer loops and proceed to bearing contact as time tends to infinity. In the experimental work, bearing contact was never experienced, a closed orbit within the clearance circle always being established. The reasons for this are not clear, though the supply pressure and groove geometry were found to be important factors and it was noted that the size of the final orbit could be reduced by increasing the supply pressure.

As the eccentricity ratio approaches unity, its first derivative approaches zero and the frequency ratio approaches 0.5, then the peak negative pressure is reduced in magnitude. Thus a reduction below the whirl onset speed and/or onset supply pressure is required to cause cavitation and thus quell any already-existing whirl. This probably accounts for the frequently observed 'hysteresis effect'.

Some interesting conclusions can be drawn from the application of a linearising technique to the oil-film forces F_1 and F_2, and using these forces to establish a frequency equation for the rigid test rotor. From this equation the frequency ratios of incipient oil-whirl instability were found and plotted in Figs. 4 and 5. The corresponding experimental plots relating to the observed limit cycles are shown in Fig.6 and show good qualitative agreement.

Whilst an uncavitated oil film promotes instability, this is not always the case for a cavitated film. Instead instability for small (ref.2) and large (ref.4) perturbations is predicted in a region defined by eccentricity ratio and P.

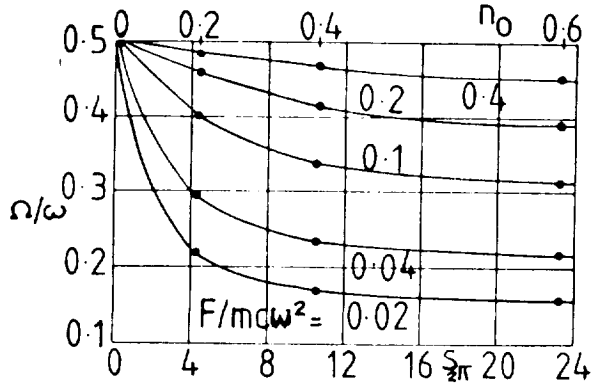

Fig.4: Short bearing

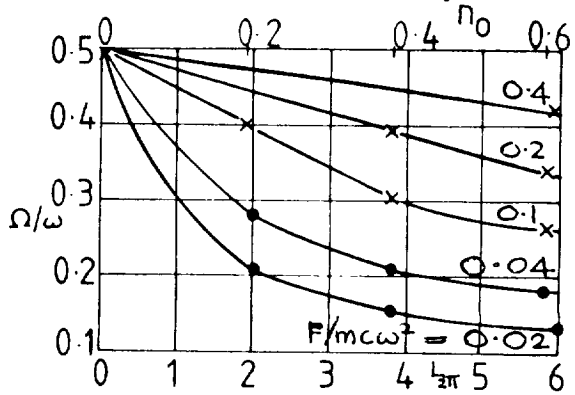

Fig. 5:Long bearing

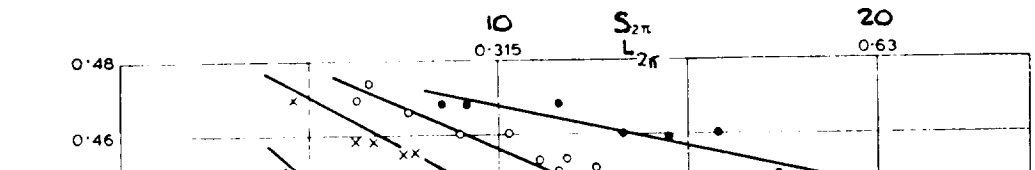

Fig.6: Experimental bearing results

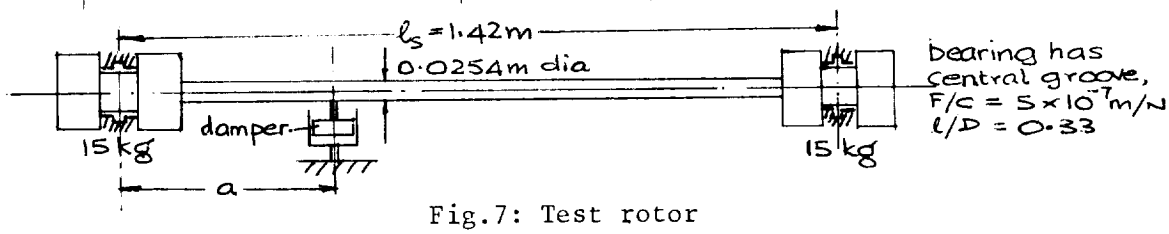

Fig.7: Test rotor

FLEXIBLE ROTOR INSTABILITY AND THE EFFECT OF EXTERNAL DAMPING

The vibrational behaviour of a flexible rotor-bearing system may be controlled by the application of external damping either directly to the rotor or by mounting the bearings on flexible, damped supports. The first option is restricted to special types of shafting, such as transmission shafts where sufficient space is available for the damping application, whereas the second option is the more attractive solution in applications such as turbomachinery where the entire length of the shaft is already occupied by discs, seals, bearings, etc.

Firstly, the effect of various parameters on the instability onset speed of the system shown in Fig.7 was examined, where external damping was included in the form of two identical viscous dampers applied at the same axial position on the shaft, one horizontally and one vertically. Later the feasibility of controlling the response and the stability of a rotor-bearing system with flexible, damped bearing supports was investigated both theoretically and experimentally.

For the first system it was found that

(a) at all values of eccentricity ratio, an increase in external damping increased the instability onset speed;
(b) at low values of eccentricity ratio ($n_o < 0.3$) the effect of external damping was fairly small;
(c) the instability onset speed increased as the damper was moved towards the centre of the span; the effect of damper location was relatively small.

An experimental rotor was built as illustrated in Fig. 7, and to minimize

external damping, the bearings had no seals and there were no axial thrust bearings. A pair of variable external dampers were mounted in the horizontal and vertical planes at one adjustable point on the shaft.

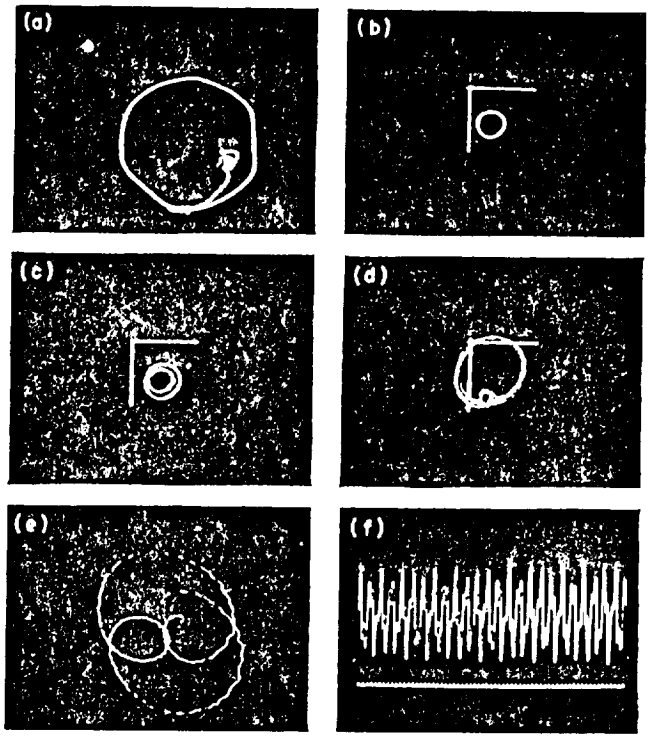

Fig.8: Experimental recordings

For running speeds below the transition range the shaft vibration was linear and harmonic, with no trace of non-synchronous vibration. Fig. 8a shows a typical motion of the journal centre, within its clearance circle, when the shaft speed was increased from zero to 250 rev/min. From its lowest position, corresponding to an eccentricity ratio of unity and a zero attitude angle, the journal acquired a stable operating position, characteristic of a cavitated oil film. Fig. 8b shows a typical journal orbit for a much higher running speed, still well below the transition range. Here the journal is performing a very small, almost circular, synchronous orbit, due to slight mass unbalance and lack of straightness of the shaft. In this figure (and in Fig. 8c and d), the horizontal and vertical lines are radius lines of the clearance circle.

For running speeds within the transition range the shaft exhibited a combination of synchronous and non-synchronous vibration, which showed no tendency to either build-up or decay with time. The non-synchronous vibration had a frequency equal to the first critical speed of the shaft (i.e. its first pinned natural frequency). Fig. 8c and d show typical journal orbits encountered when running in the upper part of the transition range. Here the bearing conditions were such that the ratio of synchronous to non-synchronous frequencies was about 2:1, which accounts for the double-loop character of the journal orbits. Another

example of a shaft orbit occurring in the transition range is shown in Fig. 8e. Here bearing conditions are such that the synchronous frequency is about three times the non-synchronous frequency. In all the cases observed it was found that, in the transition range, the journal orbits always centred on a position characteristic of a cavitated oil film, i.e. at a position well below the horizontal line through the centre of the clearance circle. This was an important observation since it showed that oil whirl did not commence as a result of the bearing oil films acquiring a full 360° extent. The complex character of the vibration in the transition range is clearly illustrated by Fig. 8f, which shows a typical variation of the horizontal component of the shaft motion with time.

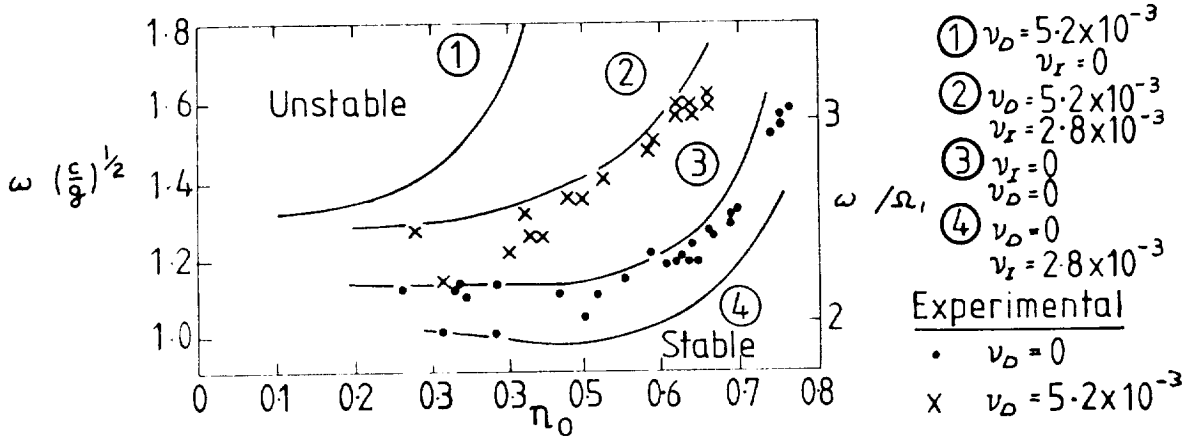

Fig.9: Instability onset speeds

For ν_D=0, that is no external damping, the experimentally determined non-dimensional instability onset speed ratios, $\omega\ (c/g)^{\frac{1}{2}}$ and $\omega\ /\Omega_1$ were plotted against n_o in Fig. 9. At high n_o it is seen that the experiments yield consistent results and the experimental scatter is small. At low n_o the scatter of the results is much greater. Also shown in Fig. 9 is the theoretically predicted variation of $\omega\ (c/g)^{\frac{1}{2}}$ with n_o ③. It is seen that, with the assumption that the internal damping is zero, a predicted curve is obtained which is in close agreement with the experimental results, shown as dots.

When the shaft is running such as to give a high eccentricity ratio (n_o = 0.75) in the bearings the threshold speed is about three times the first critical speed, Ω_1, and indeed is close to the second critical speed. Just below this threshold speed the shaft vibrates synchronously in its second bending mode. The shaft motion was measured at two locations in the horizontal plane (quarter span and three-quarter span) which corresponded to the peaks of the second mode shape. Fig. 10a shows the vibration at these points, for ω = 3300 rev/min. When the threshold speed is reached the shaft becomes unstable with a precession frequency and shape corresponding to the first mode. This is illustrated in the experimental results shown in Fig. 10b for which the same locations have been used and ω = 3350 rev/min.

It was found experimentally that even a small amount of external damping had a considerable stabilizing effect on the shaft. For example, as shown

in Fig. 9 dampers with a ν_D value of 5.2×10^{-3}, applied to the shaft (Fig.7) at $a/\ell_s = 0.2$, had the effect of substantially extending the range of experimental stable operating speeds. The onset of non-synchronous vibration was found to be more gradual than in the case of no external damping and it sometimes took several minutes for the vibration to build up. In the vicinity of the transition range the shaft was observed to be sensitive to any external disturbances, coming either from the drive unit or intentionally applied by a striker device. It was sometimes possible to create complete instability, when running in the transition range, by applying an external impulse to the shaft. However, in some cases, mainly at high eccentricity ratios, an external impulse had no tendency to promote instability.

As shown in Fig. 9 the predicted instability onset speed of the shaft,with the measured value of external damping but no internal damping is much higher than than experimentally observed, particularly at high eccentricity ratios. As the character of the internal damping and its distribution along the shaft were unknown, the simplest theoretical model was chosen, consisting of uniformly distributed, rotating viscous damping. Computations revealed that internal damping reduced the instability onset speed of the system throughout a wide range of eccentricity ratio, particularly when external damping was present. Such damping,due to shaft hysteresis and shrink fits, of the type employed in the test rig, would probably amount to a damping ratio,ν_I, between about 1 and 10×10^{-3}. In the present case this amounts to an internal damping coefficient between 1 and 10 Ns/m. Theoretical results obtained with an internal damping ratio of $\nu_I = 2.8 \times 10^{-3}$ are shown in Fig. 9, both for the case of zero external damping and for the case of an external damper with $\nu_D = 5.2 \times 10^{-3}$. It will be observed that the inclusion of internal damping in the analysis enables the agreement between theory and experiment to be considerably improved. It is recognized, however, that other factors may help to account for the discrepancy between the experimental results and the theoretical results for no internal damping.

The second rotor-bearing system used in experiments is shown in Fig. 11. It consisted of a flexible, symmetric rotor supported by two identical plain fluid-film bearings surrounded by squeeze-film isolators.

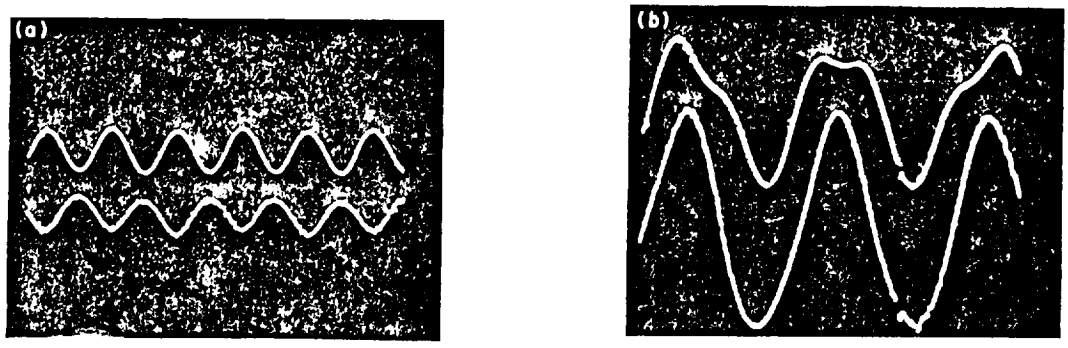

Fig. 10: Experimental recordings

Well-defined instability threshold speeds, as predicted by linear theory, were observed for large values of squeeze-film damping, while for low squeeze-film damping (below 5×10^3 N s/m), the system was stable and well damped in the entire operating speed range 0-4000 rev/min. However, in the damping

range $6 \times 10^3 - 3 \times 10^4$ N s/m, steady non-synchronous whirling commenced at a rotational speed in the region of 1740-2250 rev/min, i.e. between twice and three times the first critical speed, with the exact onset speed depending on the damping value. The non-synchronous whirl amplitude would increase with speed up to about 2400 rev/min, i.e. about three times the first critical speed, whereafter the non-synchronous whirl component amplitude would decrease rapidly and vanish at about 2400-2740 rev/min. The response would then remain synchronous up to about 2870-3230 rev/min, still depending on the particular squeeze-film damping value, where non-synchronous whirling would reappear. In some instances, again depending on the damping, the whirl amplitudes at this speed would continue to grow, indicating conventional system instability, while in other cases the amplitude grew to a maximum with increasing speed and disappeared at about 3690-3800 rev/min. Thereafter,the system would remain stable up to and including the maximum operating speed of 4000 rev/min.

With an increase in oil temperature, it was possible to eliminate the second non-synchronous whirl region, and a further temperature increase would result in the disappearance of the first whirl region also, making the system inherently stable by not allowing the journal bearing oil films to exert their full influence. However, the system remained very sensitive to random transient excitation, such as tapping of the foundation with a rubber hammer, particularly near the first whirl region, and generally appeared to be very lightly damped at all speeds above twice the first critical speed. Variations in oil supply pressure had relatively little effect. The non-synchronous whirling exhibited the well-known hysteresis effect of persisting over a wider speed range once initiated.

Fig. 12 shows examples of the non-synchronous whirl orbits in the two whirl regions. The steady-state double and triple loops indicate whirl speeds of exactly 1/3 and 1/4 of the respective rotational speeds. Only at speeds of 2430 and 3323 rev/min (corresponding to roughly three times and four times the first critical speed) were the orbits stationary. Non-synchronous whirling was never found to reappear, either experimentally or theoretically, as a result of reduction in the bearing support damping from about 1×10^4 N s/m down to the minimum value of about 200 N s/m. Both the experimental and the predicted effects of bearing support stiffness were almost negligible within the covered stiffness range of 7×10^5 down to 8.85×10^4 N/m.

CONCLUSIONS

The main conclusions of the work described in this paper can be summarised as follows.

1) For a rigid rotor running in uncavitated journal bearings a good qualitative understanding of oil-whirl instability can be obtained by utilising in turn the short and long bearing assumptions in numerical computations.

2) For a flexible rotor-bearing system it was revealed that small amounts of external damping at a position in the shaft span increase the instability onset speed and that this effect is most pronounced when the eccentricity ratio for the bearings is high. External point damping is thus a useful method

for achieving stability control.

3) Experimental work has verified the theoretical assumption that the oil films in the bearings remain cavitated, even at the threshold of instability.

4) Instability onset speeds from two up to three times the first critical speed have been achieved experimentally, by varying the bearing operating conditions.

5) Good agreement between theoretically and experimentally determined instability onset speeds has been obtained in the case of no external point damping.

6) In the case of externally applied point damping, it has been shown that the inclusion of internal damping in the analysis enables the agreement between theoretically and experimentally determined instability onset speeds to be considerably improved. Internal damping had relatively little effect when no external point damping was applied.

7) The feasibility of controlling the vibration of a rotor-bearing system by mounting the bearings on squeeze-film isolators has also been demonstrated. Both numerical predictions and experimental results show a great improvement in stability when suitable external damping is employed. Inherent stability could be obtained within a large range of isolator stiffness and damping values, while for other values nonlinear behaviour was observed over distinct speed ranges where subharmonic steady-state vibrations of orders up to four occurred.

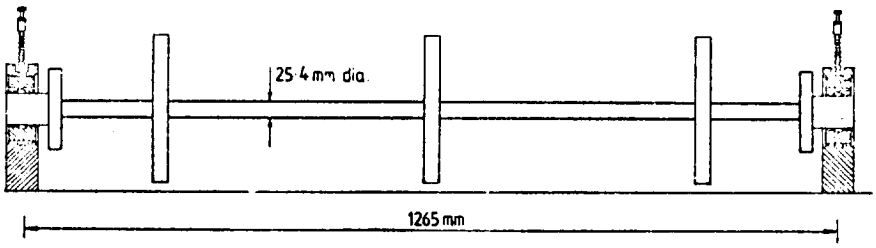

Fig. 11: Experimental system

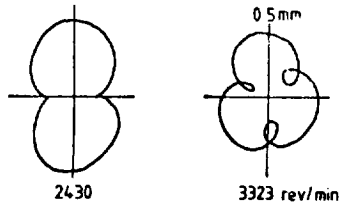

Fig.12: Non-synchronous orbits

REFERENCES

1) Holmes, R. 'Oil whirl characteristics of a rigid rotor in 360° journal bearings'., Proc. Instn Mech.Engrs. 1963, 177, (No.11), 291.

2) Holmes, R. 'The vibration of a rigid shaft on short sleeve-bearings'. Journ. of Mech. Engng Sci.,1960, 2, 337-341.

3) Swift, H.W. 'Fluctuating loads in sleeve bearings'. J. Instn. Civ.Engrs 1937, 5, 161.

4) Capriz ,G. 'Sulle vibrazioni della aste rotanti', 1963, Ann Scucla Normale Superiore, 17, 31.45.